CANCER IMMUNOLOGY

Tumor-derived antioxidants suppress immunity by depriving T cells of reactive oxygen species

Alexander J. Wesolowski[1,2]*†, Ardon M. Pillay[1,2]†, Panagiota Vardaka[3], Rabab Nasrallah[3], Randy Greaves[1,2], Housaiyin Li[1,2], Iliana Loffreda[4], Chelsea Jenkin[5], Andrew M. James[6], Alica Nübling[7], Christopher J. Ward[1], Teresa von Linde[1], Alberto G. Conti[1], Sheue-Fen Tzeng[8], Layla Dahmani[1], Alexander C. Evans[1], Sarah K. Whiteside[1], Yumi Yamashita-Kanemaru[1], Charlotte J. Imianowski[1], Jie Yang[1,9], Ignacio Moraga Gonzalez[10], Jack Chapman[1], Aws Al-Deka[1,2], Klaus Okkenhaug[1,2], Michael P. Murphy[6,11], Bartlomiej Swiatczak[1,2], Geoffrey Guittard[4], Enrico Lugli[12], Lukas Flatz[7], Ping-Chih Ho[13], Robert L. Eil[5]*‡, Rahul Roychoudhuri[1,2]*‡

Reactive oxygen species (ROS) promote genomic instability and fuel oncogenic signaling in cancer, but antioxidant therapies have so far failed to improve, or worsen, cancer outcomes. Emerging data suggest that T cells depend on ROS for signal transduction. In this study, we show that tumors exploit this dependency, releasing antioxidant enzymes into the tumor environment to suppress T cell–mediated antitumor immunity. The interstitial fluid of tumors possesses potent antioxidant activity, associated with enrichment of the antioxidant enzyme peroxiredoxin 1 (PRDX1). Extracellular PRDX1 deprives T cells of ROS, preventing oxidative inactivation of phosphatases required for T cell receptor–driven kinase signaling and effector function. *Prdx1* is up-regulated upon cancer immunoediting, and loss of PRDX1 within tumors enhances antitumor immunity and immunotherapy responses. These findings define a redox-dependent mechanism of tumor immunosuppression that is potentially amenable to therapeutic intervention.

Cancer cells exhibit dysregulated redox metabolism, characterized by increased intracellular production of reactive oxygen species (ROS), which drive genomic instability through DNA damage and sustain tumorigenic signaling (*1*, *2*). This has led to an interest in using antioxidants to prevent or treat cancer. Public use of antioxidant supplements among healthy individuals and cancer patients to counteract the perceived protumorigenic role of ROS is widespread (*3*, *4*). However, multiple large randomized controlled trials have paradoxically shown that antioxidants fail to improve or worsen cancer outcomes (*5*–*8*). These findings underscore the need to better understand how redox dynamics shape not only the biology of cancer cells but also their interactions with the host. It is increasingly evident that cancer cell–intrinsic metabolic adaptations can profoundly shape the extrinsic tumor microenvironment, with important consequences for tumor-specific immunity (*9*–*13*). However, how aberrant redox states of tumors influence antitumor immunity remains unclear.

Recent work has revealed that ROS are essential cofactors for T cell activation and differentiation (*14*–*18*). ROS are generated by cells primarily in the form of superoxide ($O_2^{\bullet-}$), which is rapidly converted to other ROS species, including hydrogen peroxide (H_2O_2), which can passively diffuse across cell membranes or through membrane aquaporins (*19*). In various cellular systems, ROS play a critical role in signal transduction, enabling kinase pathway activation by transiently inactivating cellular phosphatases through reversible oxidation of catalytic cysteines within their active sites (*20*, *21*). Upon stimulation, T cells produce extracellular ROS via plasma-membrane nicotinamide adenine dinucleotide phosphate (NADPH) oxidases (*22*), which are required for optimal T cell activation (*16*). T cells also produce mitochondrial ROS upon activation, and although this is largely dispensable for acute activation, mitochondrially derived ROS regulate T cell differentiation (*17*, *18*). Moreover, treatment of T cells with antioxidant drugs broadly restricts both T cell activation and effector programs (*14*, *15*). Thus, T cells are profoundly dependent on ROS for signal transduction and differentiation, but whether tumors exploit this dependency to suppress T cell responses is not known.

Here, we show that cancer cells release antioxidant enzymes into the tumor interstitium, creating an antioxidant extracellular environment that is suppressive of T cell activation. Peroxiredoxin 1 (PRDX1), a ROS-scavenging antioxidant enzyme that neutralizes hydrogen peroxide, is abundantly present in the extracellular environment of tumors. The addition of extracellular PRDX1 to T cells reduces intracellular ROS abundance, limiting T cell receptor (TCR)–driven kinase signaling and effector function by maintaining the activity of membrane-proximal redox-sensitive phosphatases. Cancer cells are the predominant source of PRDX1 released into the tumor interstitium across multiple models, and *Prdx1* expression is induced upon cancer immunoediting in vivo. Consequently, genetic disruption of *Prdx1* in cancer cells reduces interstitial PRDX1 abundance, enhances intratumoral T cell activation, and sensitizes tumors to antitumor immunity and immunotherapy. These findings reveal a previously unrecognized redox-dependent mechanism of tumor immunosuppression that is potentially amenable to therapeutic intervention.

Tumor interstitial fluid is highly immunosuppressive and possesses potent antioxidant activity

We initially sought to examine how the tumor interstitial environment affects T cell activation and function. To test this, we isolated tumor interstitial fluid (TIF) from tumors of mice implanted with syngeneic murine B16-F10 melanoma cells and added it to effector $CD8^+$ T cells undergoing restimulation with antibodies against CD3 (anti-CD3) in vitro. We found that TIF profoundly suppressed the production of the effector cytokine interferon-γ (IFN-γ) when added in dilute quantities during brief (4 hours) restimulation (Fig. 1A and fig. S1A). TIF isolated from subcutaneous MC38 colorectal adenocarcinomas possessed comparable suppressive activity (fig. S1B), and the suppression extended beyond IFN-γ to multiple markers of T cell activation and cytotoxicity, including tumor necrosis factor (TNF) and the degranulation marker CD107a (Fig. 1B). The suppressive activity of TIF was evident across a range of anti-CD3 concentrations (fig. S1C) and in the context of cognate peptide antigen stimulation (fig. S1D). Furthermore, the interstitial fluid isolated from lungs bearing B16-F10 metastases profoundly suppressed T cell activation when compared to interstitial fluid from healthy lungs (Fig. 1C). The suppressive activity of TIF was retained in the >10-kDa macromolecular fraction and was partially heat-labile (fig. S1, E and F). Blockade or neutralization of the immunosuppressive molecules PD-1, transforming growth factor–β (TGF-β), or CTLA-4 failed to reverse TIF-mediated suppression of T cell activation (fig. S1G). Notably, TIF isolated from *Rag2*$^{-/-}$ mice, which lack

[1]Department of Pathology, University of Cambridge, Cambridge, UK. [2]CRUK Cambridge Centre, Cambridge, UK. [3]Babraham Institute, Babraham, Cambridgeshire, UK. [4]Centre de Recherche en Cancérologie de Marseille, Marseille, France. [5]Department of Surgery, Oregon Health and Science University, Portland, OR, USA. [6]MRC Mitochondrial Biology Unit, University of Cambridge, Cambridge, UK. [7]Department of Dermatology, University of Tubingen, Tubingen, Germany. [8]Tumor Immune Analysis Core, Office of Research and Development, Taipei Medical University, Taipei, Taiwan. [9]Department of Oncology, University of Oxford, Oxford, UK. [10]Division of Cell Signaling and Immunology, University of Dundee, Dundee, UK. [11]Department of Medicine, University of Cambridge, Cambridge, UK. [12]IRCCS Humanitas Research Hospital, Rozzano, Milan, Italy. [13]Ludwig Institute of Cancer Research, University of Lausanne, Lausanne, Switzerland. ***Corresponding author. Email: ajw299@cam.ac.uk (A.J.W.); eil@ohsu.edu (R.L.E.); rr257@cam.ac.uk (R.R.)** †These authors contributed equally to this work. ‡These authors contributed equally to this work.

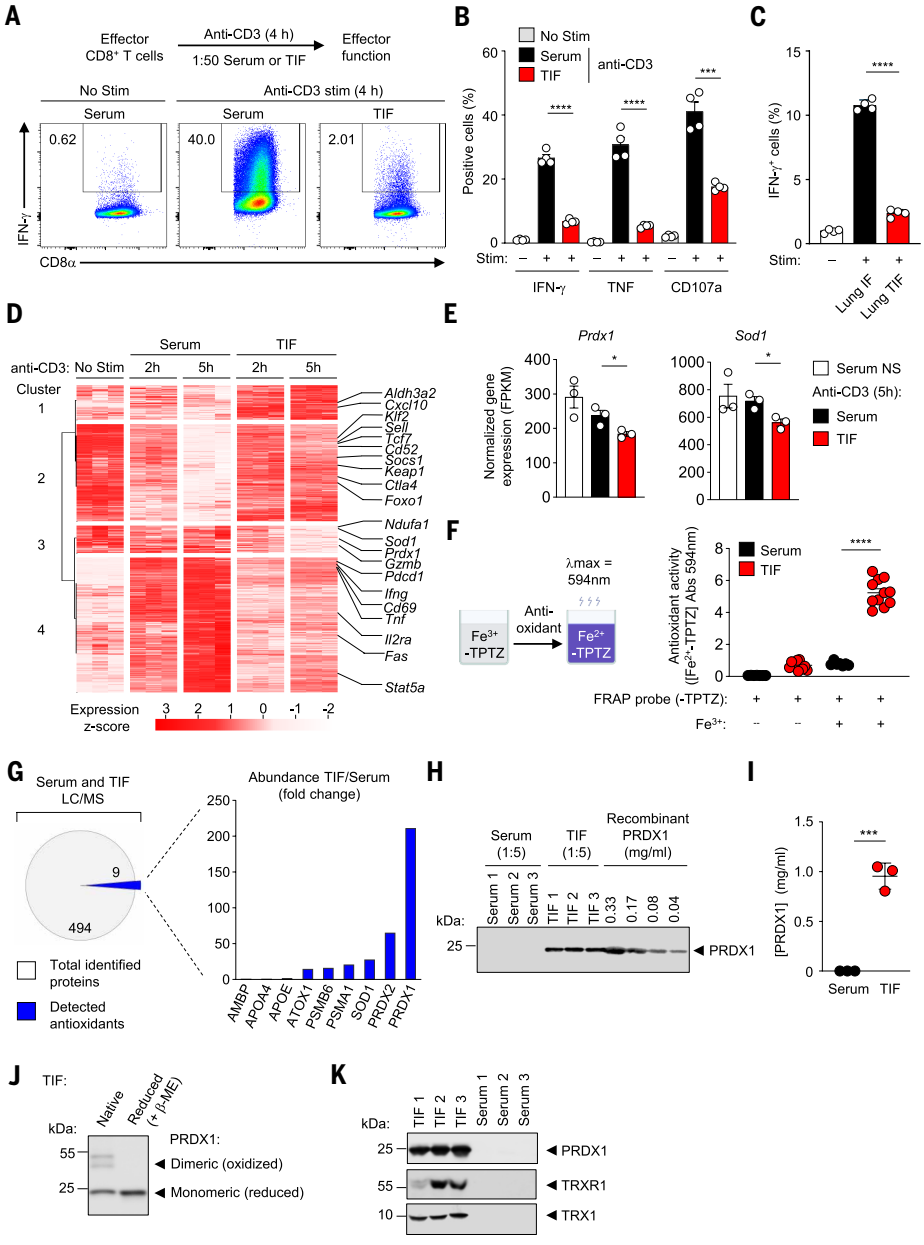

Fig. 1. The interstitial fluid of tumors suppresses T cell activation and possesses antioxidant activity. (**A**) Experimental schema (top) and representative flow cytometry plots (bottom) showing IFN-γ production by effector CD8$^+$ T cells restimulated with anti-CD3 (1 μg/ml, 4 hours) in the presence of serum or tumor interstitial fluid (TIF) (1:50 dilution). Effector CD8$^+$ T cells were harvested 4 days after primary stimulation of splenocytes from OT-I TCR^{tg} mice with cognate SIINFEKL peptide. (**B**) Quantification of IFN-γ, TNF, and CD107a expression by CD8$^+$ T cells stimulated as in (A). (**C**) Quantification of IFN-γ production by CD8$^+$ T cells stimulated with anti-CD3 (1 μg/ml, 4 hours) in the presence of lung interstitial fluid (IF) or B16-F10 metastasis-bearing lung (lung TIF), both at 1:50 dilution. (**D**) Heatmap of differentially expressed genes in CD8$^+$ T cells stimulated for 2 or 5 hours in the presence of serum or TIF [$|\log_2$FC (fold change)$| > 0$, adjusted P value (P_{adj}) ≤ 0.05]. Gene expression [row-wise z-scores of $\log_2$(FPKM + 1); fragments per kilobase of transcript per million mapped reads] hierarchically clustered by the Ward.D method. (**E**) Expression of antioxidant genes (FPKM) in CD8$^+$ T cells treated as in (D). (**F**) Schematic of ferric reducing antioxidant power (FRAP) assay reaction (left; TPTZ, 2,4,6-tripyridyl-s-triazine) with corresponding measurements of cell-free antioxidant activity in TIF versus matched serum (right); TIF $n = 12$, serum $n = 8$ biological replicates, each from separate tumors. Control reactions showing probe measurements in the absence of Fe^{3+} substrate shown. (**G**) Pie chart showing proportion of all proteins detected by mass spectrometry in serum and TIF with annotated antioxidant activity (left), and relative abundance of identified antioxidant proteins in TIF compared to serum (right); antioxidants were annotated using the AOD antioxidant protein database (*63*). (**H**) Western blot analysis of PRDX1 abundance in TIF and matched serum, alongside a recombinant PRDX1 standard curve; $n =$ three individual mice per group. (**I**) Quantification of PRDX1 concentration in TIF and serum by interpolation from the standard in (H); $n = 3$ biological replicates, as in (H). (**J**) Nonreducing SDS-PAGE of TIF isolated in the presence of NEM (50 mM), with or without β-mercaptoethanol (β-ME) reduction, showing native PRDX1 predominantly in its monomeric (reduced) form within TIF; both lanes derived from a single TIF preparation split prior to reduction. (**K**) Western blot analysis of PRDX1, thioredoxin reductase 1 (TRXR1) and thioredoxin 1 (TRX1) abundance in TIF and matched serum (1:5 dilution); $n = 3$ biological replicates per condition, from different mice than in (H); Ponceau S staining of the same membrane is shown in fig. S3F. Data in (B), (C), (E), (F), and (I) indicate mean ± SEM. (B and C) $n = 4$ technical replicates; (E) $n = 3$ technical replicates; (F) $n = 12$ (TIF) and $n = 8$ (serum) biological replicates, each from separate tumor-bearing mice; (I) $n = 3$ biological replicates [as in (H)]. All quantified data are representative of at least two independent experiments. (B) multiple unpaired two-tailed Student's t tests; (C, E, I) two-tailed unpaired Student's t test; (F) two-way analysis of variance (ANOVA) with Tukey's multiple comparisons test. *$P < 0.05$; **$P < 0.01$; ***$P < 0.001$; ****$P < 0.0001$.

adaptive immune cells, possessed similar suppressive activity to that of TIF from wild-type (WT) mice, suggesting that the suppressive activity of TIF is largely independent of molecules secreted by adaptive immune cells (fig. S1H). Thus, the tumor interstitial environment contains a heat-labile macromolecular component that potently inhibits $CD8^+$ T cell activation and effector function.

To gain broader insight into how TIF affects the $CD8^+$ T cell activation and functional program, we performed RNA sequencing (RNA-seq) of effector $CD8^+$ T cells undergoing brief restimulation in the presence of TIF or serum (data file S1). Unsupervised hierarchical clustering of TIF-regulated genes revealed several clusters of genes with distinct expression patterns (Fig. 1D; fig. S2, A to C; and data file S2). Moreover, TIF suppressed the induction of phenotypic markers associated with T cell activation and exhaustion upon restimulation of effector $CD8^+$ T cells in vitro (fig. S2D).

We observed broad suppression of stimulation-driven transcriptional programs and noted that the genes encoding PRDX1 and SOD1, potent antioxidant enzymes typically up-regulated in response to oxidative stress, were among cluster 3 genes down-regulated in the presence of TIF and unaffected by stimulation alone (Fig. 1E). Moreover, TIF treatment reduced expression of a number of NRF2 target genes typically up-regulated in response to oxidative stress (fig. S3A). This raised the possibility that T cells exposed to TIF experience reduced oxidative stress, leading us to ask whether TIF possesses antioxidant activity. To measure the antioxidant potential of TIF, we assessed its ability to reduce ferric (Fe^{3+}) ions to ferrous (Fe^{2+}) ions using the ferric reducing antioxidant power (FRAP) assay (*23*). Notably, TIF possessed substantially greater antioxidant activity than serum isolated from matched tumor-bearing mice (Fig. 1F). Similarly, interstitial fluid isolated from B16-F10 metastasis-bearing lungs possessed markedly greater antioxidant activity than interstitial fluid from healthy lungs (fig. S3B). Moreover, acute treatments with TIF resulted in decreased total and mitochondrial ROS in exposed effector $CD8^+$ T cells (fig. S3, C and D). These data led us to conclude that the interstitial environment of tumors possesses potent immunosuppressive and antioxidant activity, although the molecular basis for these properties and their functional relationship was unclear.

Antioxidant protein PRDX1 is highly enriched in the extracellular environment of tumors and suppresses T cell activation

We observed that the interstitial fluid of tumors possesses potent antioxidant activity. Proteins with antioxidant activity are present within cells and extracellular spaces and contribute to redox regulation. To determine whether TIF contains antioxidant proteins, we performed highly quantitative mass spectrometry of tandem mass tag (TMT)–labeled TIF and serum samples. Among 494 proteins detected, 9 with previously characterized antioxidant activity were identified, of which peroxiredoxin 1 (PRDX1) was the most highly enriched in TIF relative to serum (Fig. 1G and data file S3).

We confirmed the enrichment of PRDX1 within TIF by antibody staining of SDS–polyacrylamide gel electrophoresis (PAGE) Western blots, which revealed substantial enrichment of PRDX1 in TIF compared to matched serum and upon normalization to total protein, confirming that PRDX1 abundance in TIF reflects specific enrichment rather than a generalized increase in protein concentration (Fig. 1H and fig. S3, E to G). This is consistent with prior unbiased proteomic analyses of human ovarian cancer and non–small cell lung cancer TIF, which detected PRDX1 among the most enriched proteins in the tumor extracellular environment (*24*, *25*). Interpolation from a standard curve of known quantities of purified recombinant PRDX1 enabled estimation of the concentration of PRDX1 within TIF to be 0.95 mg/ml [95% confidence interval (CI), 0.62 to 1.28 mg/ml] (Fig. 1I and fig. S3H). PRDX1 cycles between a catalytically active reduced state and an inactive oxidized dimer linked by an intermolecular disulfide bond; on nonreducing SDS-PAGE these forms migrate as a monomer and covalent dimer, respectively. Nonreducing SDS-PAGE of TIF isolated in the presence of the alkylating agent *N*-ethylmaleimide (NEM), which preserves the in situ redox state of proteins by capping free thiols, revealed that PRDX1 exists predominantly in its reduced form within TIF (Fig. 1J). Furthermore, the physiological PRDX1 recycling machinery, thioredoxin 1 (TRX1) and thioredoxin reductase 1 (TRXR1), were enriched within TIF relative to matched serum (Fig. 1K). Together, these findings indicate that catalytically active PRDX1 and its recycling machinery are abundantly present in the extracellular environment of tumors.

Emerging evidence suggests that T cells are dependent upon ROS for signal transduction (*1*, *14*, *26*). We therefore asked whether the antioxidant protein PRDX1 suppresses $CD8^+$ T cell activation when present in the extracellular space. Notably, the addition of purified recombinant PRDX1 to effector T cells during acute (4 hours) restimulation profoundly suppressed the production of effector cytokines and cytotoxic molecules (Fig. 2A and fig. S4A), a finding reproduced across multiple independent PRDX1 preparations (fig. S4B). Consistent with its known antioxidant activity, PRDX1 treatment led to a reduction in both total cellular and mitochondrial ROS (Fig. 2, B and C, and fig. S4, C to E). PRDX1 had minimal effect on cellular GSH:GSSG, NAD^+:NADH, or $NADP^+$:NADPH ratios, reflecting the large buffering capacity of these cofactor pools (fig. S4F). Notably, IFN-γ production was enriched within the $MitoSOX^{high}$ population, and PRDX1 treatment reduced the frequency of $MitoSOX^{high}$ cells; the PRDX1-driven difference in IFN-γ production was minimized upon separate analysis of $MitoSOX^{high}$ and $MitoSOX^{low}$ cells, indicating that the reduction in mitochondrial ROS and loss of effector function upon PRDX1 treatment are associated (fig. S4, H to J).

Consistent with the antioxidant activity of PRDX1 underpinning its ability to suppress IFN-γ production during T cell restimulation, we observed similar suppression of T cell activation by widely used antioxidant *N*-acetyl cysteine (NAC) (Fig. 2D). Likewise, treatment of cells with PRDX1 or NAC suppressed stimulation-driven T cell proliferation (Fig. 2E). Intracellular redox systems, including the lipid peroxidation, glutathione, and thioredoxin pathways, are coupled through shared dependence on reducing equivalents, such that perturbation of one pathway can alter flux through others (*21*). We observed that ferrostatin-1, an inhibitor of lipid peroxidation, suppressed IFN-γ production by effector $CD8^+$ T cells in a dose-dependent manner (fig. S4G), collectively revealing convergent immunosuppressive effects of mechanistically diverse antioxidants.

To determine whether the suppressive activity of PRDX1 is dependent upon extracellular ROS depletion, we asked whether enhancing extracellular ROS production in T cell cultures overcomes PRDX1-mediated suppression of T cell activation. To achieve this, we overexpressed the extracellular ROS-producing NADPH oxidase component NOX1 in T cells using retroviral transduction before restimulating these T cells in the presence or absence of extracellular PRDX1. NOX1 overexpression in the absence of PRDX1 drove supraphysiological cytokine production, whereas NOX1 overexpression in the presence of PRDX1 restored cytokine production to baseline levels (Fig. 2F). The addition of extracellular PRDX1 suppressed cytokine production to a comparable extent in both control and NOX1-overexpressing T cells (1.46- and 1.39-fold reductions, respectively). These findings suggest that T cells exist along a functional continuum determined by the balance of extracellular antioxidants and pro-oxidants.

To better understand the impact of extracellular PRDX1 on the T cell activation program, we performed RNA-seq analysis of effector T cells acutely restimulated in the presence of PRDX1 (data file S4). In accordance with our proteomic data, treatment of T cells with PRDX1 suppressed the stimulation-driven induction of multiple genes involved in effector function, including *Gzmb*, *Ifng*, and *Il2*, as well

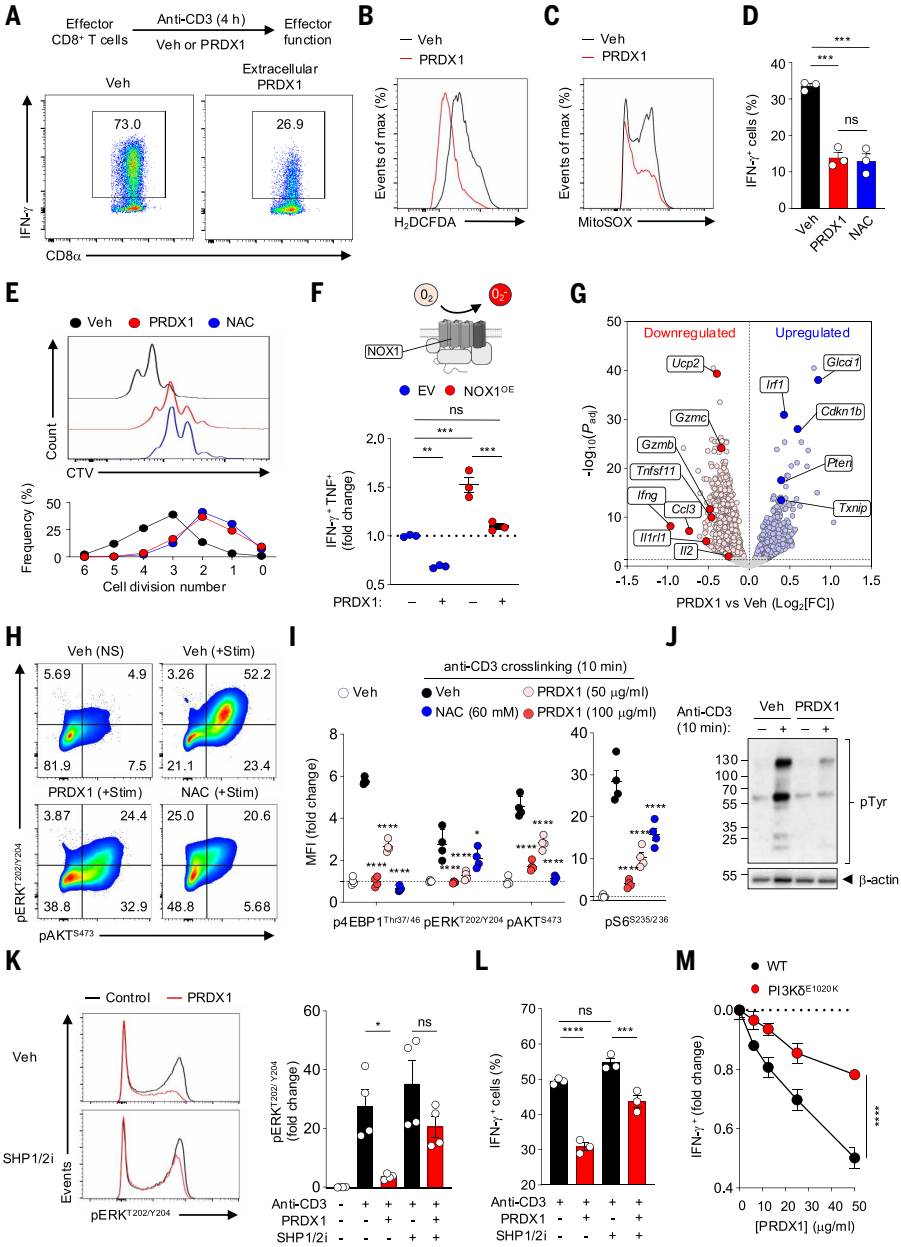

Fig. 2. Extracellular PRDX1 suppresses T cell activation by scavenging ROS and limiting kinase signaling. (**A**) Experimental schema (top) and representative flow cytometry plots (bottom) showing IFN-γ production by effector CD8$^+$ T cells restimulated for 4 hours with anti-CD3 (1 μg/ml) in the presence of extracellular recombinant PRDX1 (25 μg/ml) or vehicle control. Effector CD8$^+$ T cells for the assay were harvested 4 days after primary stimulation of splenocytes from OT-I TCRtg mice with cognate SIINFEKL peptide. (**B** and **C**) Representative histograms of total cellular ROS (H_2DCFDA) (B) and mitochondrial ROS (MitoSOX) (C) in CD8$^+$ T cells treated for 4 hours with PRDX1 (25 μg/ml) or vehicle control, quantified in fig. S4, C and E, respectively. (**D**) Quantification of IFN-γ$^+$ frequency in CD8$^+$ T cells stimulated with anti-CD3 (1 μg/ml, 4 hours) in the presence of vehicle, recombinant PRDX1 (25 μg/ml) or *N*-acetylcysteine (NAC, 80 mM). (**E**) Representative histograms (top) and quantification (bottom) of CellTrace Violet (CTV) dilution in CD8$^+$ T cells stimulated for 3 days in the presence of vehicle, PRDX1 (50 μg/ml), or NAC (40 mM). (**F**) Schematic outlining ROS production by NADPH oxidases (top) and IFN-γ$^+$ TNF$^+$ frequency (bottom) of effector T cells retrovirally transduced with NOX1 or empty vector (EV) control and subsequently restimulated with anti-CD3 (1 μg/ml, 4 hours) in the presence of recombinant PRDX1 (50 μg/ml) or vehicle control. Fold changes are normalized to the mean of empty vector–transduced vehicle-treated T cells. (**G**) Volcano plot showing differentially expressed genes in effector CD8$^+$ T cells restimulated with anti-CD3 (1 μg/ml, 4 hours) in the presence of PRDX1 (50 μg/ml) or vehicle control. (**H**) Representative flow cytometry plots of phosphorylation at AKT^{S473} and ERK$^{T202/Y204}$ residues after stimulation with cross-linked anti-CD3 (10 min) in the presence of PRDX1 (100 μg/ml), NAC (60 mM), or vehicle control. (**I**) Fold change median fluorescence intensity (MFI) (relative to unstimulated Veh) of indicated residues in CD8$^+$ T cells after anti-CD3 cross-linking (10 min) under the conditions indicated. (**J**) Immunoblot of global phosphotyrosine (pTyr) in CD8$^+$ T cells after anti-CD3 cross-linking (10 min) in the presence of Veh or PRDX1 (50 μg/ml). (**K**) Representative histograms (left) and quantification (fold change relative to unstimulated Veh) (right) of pERK$^{T202/Y204}$ phosphorylation in CD8$^+$ T cells after anti-CD3 cross-linking (5 min) in the presence of PRDX1 (50 μg/ml) with or without SHP1/2 inhibition (NSC-87877, 4 μM). (**L**) Quantification of IFN-γ$^+$ frequency of CD8$^+$ T cells stimulated with anti-CD3 (1 μg/mL, 4 hours) in the presence of vehicle or PRDX1 (50 μg/mL) with or without SHP1/2 inhibition (NSC-87877, 4 μM). (**M**) Quantification of IFN-γ$^+$ frequency (fold change relative to 0 μg/ml PRDX1 within each genotype) in wild-type or PI3Kδ^{E1020K} effector CD8$^+$ T cells restimulated with anti-CD3 (1 μg/ml, 4 hours) in the presence of PRDX1 at the indicated concentrations. Data indicate mean ± SEM of (D, F, L, M) $n = 3$ technical replicates; (E, I, K) $n = 4$ technical replicates. All quantified data are representative of at least two independent experiments. (D, F, I, K, L) one-way ANOVA with Tukey's multiple comparisons test; (M) ordinary two-way ANOVA. *$P < 0.05$; **$P < 0.01$; ***$P < 0.001$; ****$P < 0.0001$; ns, not significant.

as the oxidative stress response genes *Prdx1* and *Sod1* (Fig. 2G and fig. S5A). Gene set enrichment analysis (GSEA) of global transcriptional changes induced by PRDX1 treatment revealed a downregulation of transcriptional programs associated with T cell activation and TCR signaling (fig. S5, B to E). The transcriptional changes induced by PRDX1 treatment were modestly correlated with those induced by both NAC and TIF treatment, suggesting commonalities in their mechanism of T cell suppression (fig. S6, A and B, and data file S5).

In multiple cellular systems, ROS promote kinase signaling by reversibly oxidizing catalytic cysteine residues in phosphatases, thereby inhibiting their activity (*27*, *28*). In T cells, TCR-driven ROS generation leads to oxidation and inactivation of membrane-proximal phosphatases including SHP-2, permitting sustained signal-driven kinase pathway activation (*29*). This led us to hypothesize that PRDX1-mediated ROS scavenging limits oxidative inactivation of phosphatases required for sustained kinase pathway activation downstream of TCR signaling. Consistent with this hypothesis, the addition of either PRDX1 or NAC to T cells markedly diminished stimulation-driven phosphorylation of S6, AKT, ERK, and 4EBP1 and suppressed global tyrosine and serine-threonine phosphorylation upon anti-CD3 cross-linking, whereas proximal signaling events, including phosphorylation of LAT and SHP1, were not reduced (Fig. 2, H to J, and fig. S7, A to D). The preservation of proximal signaling suggests that PRDX1 does not impede extracellular receptor engagement or initial TCR triggering, but rather acts to restrain downstream signal amplification. The preservation of proximal signaling is consistent with multiple independent studies demonstrating that SHP2, whether constitutively activated by gain-of-function mutation or by deletion of its autoinhibitory SH2 domains, does not alter phosphorylation of TCR ζ chain, ZAP-70, or LAT in T cells (*30*–*32*). Rather, SHP2 appears to act on effectors downstream of these proximal components. Accordingly, pharmacological inhibition of SHP-1/2 limited the ability of PRDX1 to suppress stimulation-driven $ERK^{T202/Y204}$ and AKT^{S473} phosphorylation (Fig. 2K and fig. S8A), and the ability of both PRDX1 and TIF to suppress IFN-γ production (Fig. 2L and fig. S8B).

Our results suggested that PRDX1 suppresses T cell activation by maintaining phosphatase activity, which subsequently restricts downstream kinase signaling. To test whether constitutive activation of a kinase pathway downstream of TCR-proximal phosphatases confers resistance to PRDX1, we used mice carrying a germline gain-of-function mutation in PI3Kδ, termed $PI3K\delta^{E1020K}$ (*33*, *34*). We observed that PI3Kδ hyperactivation confers significant resistance to PRDX1- and TIF-mediated suppression suggesting that PRDX1 and TIF suppress T cell activation through inactivation of TCR-driven kinase signaling (Fig. 2M and fig. S8C) (*33*, *34*). We had noted that treatment with PRDX1 down-regulated gene sets associated with mitochondrial oxidative phosphorylation (fig. S5E). Addition of extracellular PRDX1 to $CD8^+$ T cells during stimulation caused a mild increase in glucose uptake, potentially reflecting a compensatory shift toward glycolytic metabolism (fig. S8D). Collectively, these findings demonstrate that extracellular PRDX1 potently inhibits T cell activation by scavenging ROS, thereby preserving the activity of the membrane-proximal phosphatases including SHP1/2, which oppose TCR-induced kinase signaling.

Cancer cells are the predominant source of extracellular PRDX1 in the tumor interstitium

Our data showed that extracellular PRDX1 potently limits T cell signal transduction and activation in vitro. To determine the cellular source of PRDX1 in the interstitial environment of tumors in vivo, we generated WT and $Prdx1^{-/-}$ cancer lines using CRISPR-Cas9, electroporating cancer cells with nontargeting control or *Prdx1*-targeting single guide RNAs (sgRNAs) complexed with Cas9 protein, respectively. Clonally derived $Prdx1^{-/-}$ B16-F10, YUMM2.1, and MC38 cells exhibited complete loss of PRDX1 protein compared to WT cells (fig. S9, A). Notably, TIF extracted from subcutaneously implanted $Prdx1^{-/-}$ tumors contained substantially reduced concentrations of PRDX1, demonstrating that cancer cells are the principal source of PRDX1 in the tumor interstitium across all models tested (Fig. 3, A to C, and fig. S9, B to D). Moreover, loss of PRDX1 was associated with a reduction in the ability of TIF to suppress acute T cell activation (fig. S9E), despite likely pleiotropic mechanisms of TIF-mediated suppression.

The release of PRDX1 into the extracellular environment by cancer cells was not restricted to murine tumors. Analysis of secretomes from 23 human cancer cell lines spanning 11 cancer types using nano–liquid chromatography–tandem mass spectrometry (LC-MS/MS) (*35*) identified a range of antioxidant proteins released by cancer cells, with PRDX1 being the most abundant in all but one model (MDA-MB-435S) (Fig. 3D and fig. S10A). Given that PRDX1 is released by cancer cells, we investigated whether *PRDX1* expression is dysregulated in human cancers. We analyzed bulk transcriptional profiles of tumors and matched adjacent normal tissue from patients in 21 cancer types represented in The Cancer Genome Atlas (TCGA). Of these, we noted that *PRDX1* mRNA expression is significantly up-regulated in tumor tissue compared with adjacent normal tissue in most cancer types (14 of 21 cancer types; $P < 0.05$), whereas it was significantly down-regulated in 4 cancer types ($P < 0.05$) and not significantly different in the remaining histologies (Fig. 3E). Complementing these findings, measurement of PRDX1 abundance in TIF and matched serum samples from two patients with melanoma revealed a substantially higher PRDX1 abundance within TIF compared with patient-matched serum (Fig. 3F), and that a greater proportion of PRDX1 in serum than in TIF was found in its inactive hyperoxidized, sulfonic acid form (fig. S10B). Analysis of previously generated single-cell RNA sequencing (scRNA-seq) data revealed *PRDX1* mRNA expression across multiple cell types within tumors, although its expression was substantially higher in malignant cells than in nonmalignant cells when grouped together according to their relative abundance in both human and mouse tumors (Fig. 3G and fig. S10, C to E) (*36*, *37*). To evaluate the impact of extracellular PRDX1 on human T cell activation, we isolated human $CD8^+$ T cells from peripheral blood and then stimulated and differentiated them into effector cells before acute restimulation in the presence of PRDX1. As in the murine context, human T cells were similarly sensitive to the suppressive effect of extracellular PRDX1 (Fig. 3H).

Cancer immunoediting is a process by which cancer cells adapt under selective pressure from immune attack (*38*). The observation that *PRDX1* mRNA is up-regulated in human cancers compared to their normal tissue of origin and that PRDX1 protein suppresses T cell activation when released by tumors into the extracellular space led us to ask whether its expression is up-regulated upon cancer immunoediting. We found that expression of *Prdx1* mRNA was increased in immunoedited versus nonimmunoedited melanoma cell lines derived from tumors of WT and *Rag1*-deficient $Braf^{fl\text{-}V600E}$ $Pten^{fl/fl}$ Tyr^{CreER} mice administered 4-hydroxytamoxifen (4-HT) on the skin surface (Fig. 3I) (*39*). Moreover, *Prdx1* mRNA was increased among immunoedited versus nonimmunoedited hepatocellular carcinoma cell lines derived from tumors of WT and *Rag1*-knockout mice induced by hydrodynamic injection of *pT3-N90-CTNNB1*, *px330-sgPTEN1*, *px330-sgPTEN2*, and *SB13* transposase-encoding plasmid vectors as previously described (*39*) (Fig. 3J). Beyond carcinogenesis, tumors can undergo further immunoediting upon checkpoint blockade immunotherapy. However, we did not observe an increase in *PRDX1* mRNA or protein abundance after checkpoint blockade immunotherapy of human and mouse melanoma tumors, respectively (fig. S10, F to H) (*40*). These findings suggest that up-regulation of *Prdx1* expression is a feature of cancer immunoediting during carcinogenesis, promoting the ability of cancer cells to evade adaptive immunity.

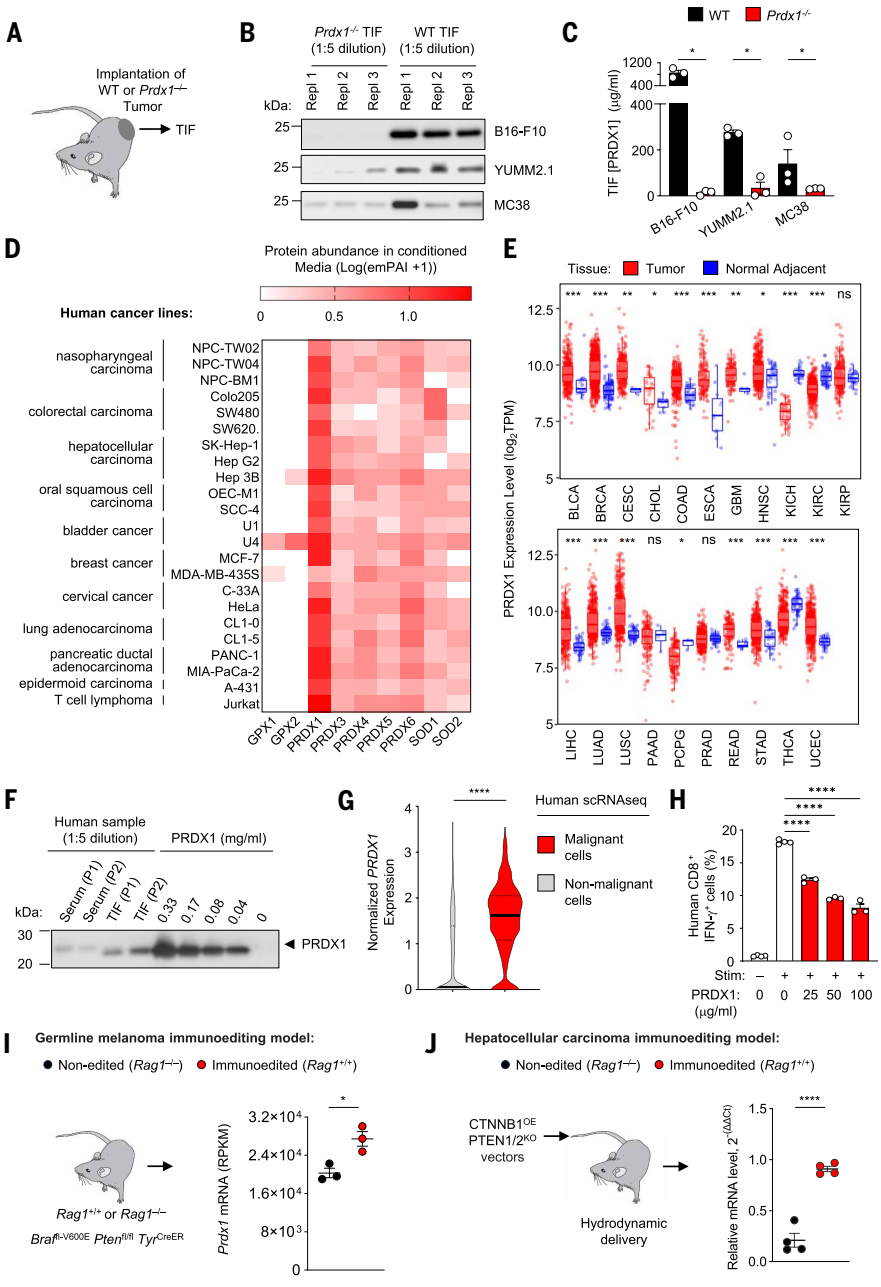

Fig. 3. PRDX1 is released into the extracellular environment by mouse and human cancer cells and is up-regulated upon cancer immunoediting. (**A**) Schematic depicting TIF isolation from subcutaneously implanted WT or *Prdx1*$^{-/-}$ tumors. (**B**) Representative immunoblot of PRDX1 in TIF (1:5 dilution) from WT and *Prdx1*$^{-/-}$ B16-F10, YUMM2.1, and MC38 tumors; $n = 3$ biological replicates per condition. (**C**) PRDX1 concentration in TIF from WT and *Prdx1*$^{-/-}$ tumors of the indicated models, quantified by densitometry against the PRDX1 standard in (B); a recombinant PRDX1 standard curve was run on each blot and used for quantification; $n = 3$ biological replicates per condition. (**D**) Heatmap showing the abundance of the indicated antioxidant proteins, log-transformed [log(emPAI + 1)], in the conditioned media of 23 human cancer cell lines spanning 11 cancer types, determined by nano-LC-MS/MS (*35*). (**E**) *PRDX1* expression ($\log_2$TPM) in tumor and adjacent normal tissue across 21 cancer types in The Cancer Genome Atlas (TCGA), analyzed using TIMER2.0; cancer types were selected on the basis of data availability for both tumor and adjacent normal tissue; Wilcoxon rank-sum test per cancer type. (**F**) Immunoblot of PRDX1 in TIF and matched serum from two patients with conventional melanoma (P1) and spindle cell malignant melanoma (P2), alongside a PRDX1 standard curve (0 to 0.33 mg/ml). (**G**) Normalized *PRDX1* mRNA expression in malignant versus nonmalignant cells from single-cell RNA sequencing (scRNA-seq) of human tumors (*37*). (**H**) Quantification of IFN-γ^+ frequency in in vitro–expanded peripheral blood CD8$^+$ T cells from a healthy donor, restimulated with anti-CD3 (1 μg/ml, 4 hours) in the presence of the indicated concentrations of PRDX1 or vehicle. (**I**) Schematic (left) and *Prdx1* mRNA expression (reads per kilobase of transcript per million mapped reads, RPKM; right) in immunoedited versus nonimmunoedited melanoma cell lines derived from tumors arising in *Braf*$^{fl\text{-}V600E}$ *Pten*$^{fl/fl}$ *Tyr*^{CreER} mice on an immunocompetent (*Rag1*$^{+/+}$) or immunodeficient (*Rag1*$^{-/-}$) background (*39*). (**J**) Schematic (left) and relative *Prdx1* mRNA expression ($2^{-(\Delta\Delta Ct)}$, right) in immunoedited versus nonimmunoedited hepatocellular carcinoma cell lines derived from tumors induced by hydrodynamic delivery of CTNNB1^{OE} and PTEN1/2^{KO} vectors into *Rag1*$^{+/+}$ or *Rag1*$^{-/-}$ mice; quantitative reverse transcription–polymerase chain reaction; $n = 4$ spontaneous tumor cell lines per background. Data in (C), (H), (I), and (J) indicate mean ± SEM of (C) $n = 3$ biological replicates per condition; (H) $n = 3$ technical replicates from one representative donor; (I and J) $n = 4$ spontaneous tumor cell lines per background. (C, H) representative of at least two independent experiments. (C) One-tailed Mann-Whitney U test per model; (E) Wilcoxon rank-sum test per cancer type; (G) Mann-Whitney U test; (H) one-way ANOVA with Dunnett's multiple comparisons test; (I and J) unpaired two-tailed Student's *t* test. *$P \leq 0.05$; **$P < 0.01$; ***$P < 0.001$; ****$P < 0.0001$; ns, not significant.

Tumor-derived PRDX1 limits T cell–mediated antitumor immunity and responses to immune checkpoint blockade

The observation that PRDX1 potently suppresses T cell function in vitro and is up-regulated in cancer cells upon cancer immunoediting in vivo led us to test the contribution of PRDX1 to tumor immunosuppression in vivo. We first asked whether PRDX1 contributes to immune suppression using the highly immunogenic YUMM2.1 melanoma line, which harbors clinically relevant genetic alterations modeling key driver mutations found in human melanoma (*41*). CRISPR-generated *Prdx1*$^{-/-}$ YUMM2.1 melanoma tumors exhibited markedly reduced growth compared to WT (NTC) controls, leading to tumor rejection that was fully reversed by depletion of CD4$^+$ and CD8$^+$ T cells (Fig. 4A).

B16-F10 melanoma cells establish immunologically "cold" tumors and are typically nonresponsive to immune checkpoint blockade with anti-PD-1 and anti-CTLA-4 antibodies in the absence of other interventions. Genetic deletion of *Prdx1* in B16-F10 melanoma cells did not impair growth rate in vitro or upon subcutaneous implantation in vivo (fig. S11, A and B). However, genetic deletion of *Prdx1* sensitized B16-F10 melanomas to immune checkpoint blockade (ICB) with anti-PD-1 and anti-CTLA-4 antibodies, and this effect was T cell–dependent as it was abolished upon combined antibody depletion of CD4$^+$ and CD8$^+$ T cells (Fig. 4B and fig. S11, C to E).

In addition, PRDX1 deficiency reduced growth of heterotopic PM299L hepatocellular carcinomas, and this effect was potentiated by ICB with anti-PD-1 and anti-CTLA-4 antibodies (Fig. 4C). However, growth of MC38 colorectal adenocarcinoma tumors was unaffected by PRDX1 loss both in untreated and anti-PD-1-treated animals, suggesting that the suppressive contribution of PRDX1 is limited to specific tumors (fig. S11F). These results show that tumor-derived PRDX1 suppresses T cell–mediated antitumor immunity and/or immunotherapy responses across multiple tumor models with distinct genetic drivers and immunogenicity profiles.

To better understand the basis for enhanced antitumor immunity and immunotherapy responses of *Prdx1*-deficient tumors, we analyzed the phenotype and function of tumor-infiltrating T cells using high-dimensional flow cytometry. Analysis of the immune infiltrate of *Prdx1*-deficient YUMM2.1 tumors revealed CD8$^+$ T cells expressing higher levels of the activation markers CD44 and CD69 (Fig. 4D) and the proliferation marker K_i-67 (Fig. 4E). Associated with heightened activation and enhanced T cell–dependent tumor control, increased frequencies of T cells from *Prdx1*-deficient tumors expressed effector cytokines, including IFN-γ and IL-2 upon ex vivo restimulation (Fig. 4, F and G). To understand the basis for heightened immunotherapy responsiveness of *Prdx1*-deficient B16-F10 tumors, we analyzed the immune phenotype of WT and *Prdx1*-deficient B16-F10 tumors treated with ICB. High-dimensional flow cytometry analysis enabled visualization of 12 FlowSOM metaclusters whose relationship and marker expression profiles could be visualized using uniform manifold approximation and projection (UMAP) dimensionality reduction (Fig. 4, H and I, and data file S6). Consistent with increased T cell signal transduction, ICB of mice bearing *Prdx1*-deficient tumors triggered the relative expansion of highly activated and proliferative CD8$^+$ T cells in clusters 5 and 6, marked by high expression of molecules associated with T cell activation and exhaustion, including CD44, CD25, and PD-1 (Fig. 4, J and K, and fig. S11, G and H). In line with increased efficacy, ICB of *Prdx1*-deficient tumors resulted in greater CD8$^+$ T cell polyfunctionality, including increased production of the effector molecules granzyme B and IFN-γ upon ex vivo restimulation (Fig. 4, L and M).

This study identifies a previously unrecognized axis of immune suppression whereby cancer cells condition their extracellular environment through the release of antioxidant proteins to deprive infiltrating T cells of ROS that serve as critical cofactors for their activation. The antioxidant enzyme PRDX1 is up-regulated upon immunoediting, abundantly released by multiple cancer models, and highly enriched in the TIF of both murine and human melanomas. Supplementation of recombinant PRDX1 at pathophysiological concentrations into the extracellular environment of T cells reduced intracellular ROS within T cells and potently suppressed T cell activation by limiting stimulation-driven kinase signaling. The suppressive effects of PRDX1 were limited by overexpression of the extracellular ROS-generating NADPH oxidase NOX1 and were dependent on the activity of SHP family protein tyrosine phosphatases, suggesting that extracellular PRDX1 regulates membrane-proximal redox-sensitive phosphatases through local peroxide scavenging. This conforms to the emerging paradigm that ROS accumulation enables TCR signal transduction by reversibly inhibiting cellular phosphatases that maintain homeostatic control (*1*, *14*, *15*, *27*). Genetic ablation of *Prdx1* in cancer cells substantially reduced interstitial abundance of PRDX1, restricted primary tumor growth in a T cell–dependent manner, and sensitized otherwise unresponsive tumors to combined anti-PD-1 and anti-CTLA-4 immunotherapy. The release of antioxidants by cancer cells to deprive T cells in the tumor environment of ROS is analogous to the involvement of Warburg metabolism in depriving T cells of environmental glucose (*42*, *43*), contributing to a broader understanding of how cancer cell metabolic rewiring generates an extracellular environment hostile to immune function. Recent studies have shown that the metabolite composition of the tumor extracellular environment differs substantially from that of the circulation (*44*). Our findings extend this framework by demonstrating that tumor-derived proteins enriched within TIF, including PRDX1 and its recycling machinery, actively reshape the redox landscape of the tumor interstitium to further impair antitumor immunity.

Collectively, our data alongside earlier studies point to the presence of a paramembranous ROS "signalosome" required to control the threshold for T cell activation. T cells produce extracellular ROS from plasma membrane NADPH oxidases upon TCR engagement (*16*, *22*), with aquaporin channels permitting their reentry into the cytosol to act on membrane-proximal phosphatases such as SHP-2, which are reversibly inactivated by oxidation of their catalytic cysteines (*19*, *29*). Because phosphatase inactivation may relieve inhibition of the same receptor-proximal kinases that drive oxidase activation, such elements may thereby form an autocrine feedback loop that potentiates signal transduction. The importance of extracellular ROS in this paramembranous autocrine signaling loop may render it particularly susceptible to interception by released antioxidant proteins.

Despite widespread interest in targeting oxidative stress in cancer, antioxidant therapies have largely failed to demonstrate clinical benefit (*5*, *6*, *45*). Furthermore, antioxidant administration in preclinical models has been associated with accelerated tumor growth and enhanced metastatic potential (*46*–*51*). Indeed, cancers with NRF2 activation are associated with immunologically cold phenotypes and poor response to cancer immunotherapy (*52*–*54*). Although ROS have roles in suppressing antimetastatic immunity in some contexts, our findings show that within the solid tumor environment, tumor-infiltrating lymphocytes (TILs) are dependent on ROS for activation, and systemic antioxidant therapies may inadvertently impair antitumor immunity and promote tumor progression.

PRDX1 lacks a classical signal peptide and is not secreted via the conventional endoplasmic reticulum–Golgi pathway. Nonclassical secretion mechanisms have been described, including exosomal release requiring oxidation-dependent dimerization (*55*); however, the predominantly reduced, monomeric state of PRDX1 within TIF suggests this may not be the primary route of secretion. Rather, given the high intracellular abundance of peroxiredoxins, passive release from dying tumor cells likely contributes to the extracellular abundance of PRDX1 in the tumor interstitium.

The presence of an immunosuppressive extracellular thioredoxin-peroxiredoxin antioxidant system in the interstitial environment of tumors raises the prospect of therapeutic intervention. Selective approaches to disrupt this axis could include drug inhibitors of extracellular PRDX1, inhibition of extracellular thioredoxin-mediated

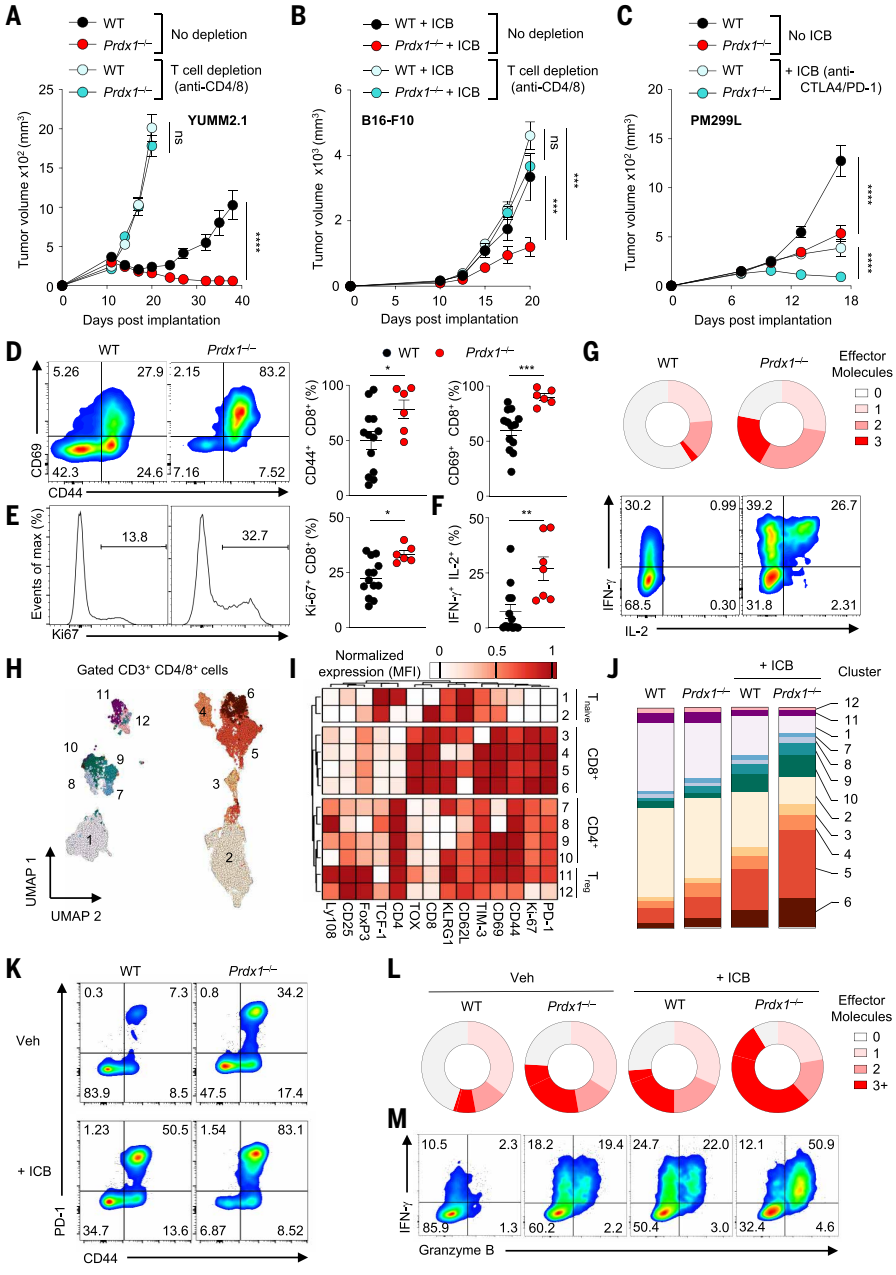

Fig. 4. Tumor-derived PRDX1 limits T cell-mediated antitumor immunity and response to immune checkpoint blockade. (**A**) Tumor growth of subcutaneously implanted WT and *Prdx1*$^{-/-}$ YUMM2.1 melanoma tumors in mice receiving no depletion or combined anti-CD4 and anti-CD8 T cell–depleting antibodies. (**B**) Tumor growth of WT and *Prdx1*$^{-/-}$ B16-F10 tumors in mice treated with anti-PD-1 and anti-CTLA-4 immune checkpoint blockade (ICB), with or without combined anti-CD4 and anti-CD8 T cell depletion. (**C**) Tumor growth of WT and *Prdx1*$^{-/-}$ PM299L hepatocellular carcinoma tumors, untreated (no ICB) or treated with anti-PD-1 and anti-CTLA-4 ICB. (**D**) Representative flow cytometry plots (left) and quantification (right) of CD44$^+$ and CD69$^+$ frequencies among tumor-infiltrating CD8$^+$ T cells from WT and *Prdx1*$^{-/-}$ YUMM2.1 tumors; $n = 13$ (WT) and $n = 6$ (*Prdx1*$^{-/-}$) mice from a single experiment. (**E**) Representative histogram (left) and quantification (right) of K_i-67$^+$ frequency among tumor-infiltrating CD8$^+$ T cells from WT and *Prdx1*$^{-/-}$ YUMM2.1 tumors; *n* as in (D). (**F**) Frequency of IFN-γ$^+$IL-2$^+$ double-positive CD8$^+$ T cells after ex vivo restimulation of tumor-infiltrating lymphocytes from WT and *Prdx1*$^{-/-}$ YUMM2.1 tumors; *n* as in (D). (**G**) Polyfunctionality of tumor-infiltrating CD8$^+$ T cells from WT and *Prdx1*$^{-/-}$ YUMM2.1 tumors, presented as donut charts of the proportion expressing 0, 1, 2, or 3 of the effector molecules IFN-γ, IL-2, and granzyme B after ex vivo restimulation (top), with representative IFN-γ versus IL-2 flow plots (bottom). (**H**) Uniform manifold approximation and projection (UMAP) of live CD3$^+$CD4$^+$ or CD3$^+$CD8$^+$ T cells from WT and *Prdx1*$^{-/-}$ B16-F10 tumors, untreated or treated with anti-PD-1 and anti-CTLA-4 ICB, analyzed by high-dimensional spectral flow cytometry. (**I**) Heatmap of median marker expression (left) across 12 clusters identified by FlowSOM clustering. (**J**) Stacked bar representation of cluster frequencies from (I) across the four conditions; quantification of clusters 5 and 6 is shown in fig. S11G. (**K**) Representative flow cytometry plots of PD-1 and CD44 expression on bulk CD8$^+$ T cells from WT and *Prdx1*$^{-/-}$ B16-F10 tumors, untreated or treated with ICB; quantification of PD-1$^+$CD44$^+$ and CD25$^+$ frequencies is shown in fig. S11H. (**L**) Polyfunctionality of CD8$^+$ T cells from WT and *Prdx1*$^{-/-}$ B16-F10 tumors, untreated (Veh) or treated with ICB, presented as donut charts of the proportion expressing 0, 1, 2, or 3+ of the effector molecules IFN-γ, TNF, IL-2, and granzyme B after ex vivo restimulation. (**M**) Representative flow cytometry plots of granzyme B and IFN-γ expression in CD8$^+$ T cells after ex vivo restimulation of tumor-infiltrating lymphocytes from the conditions in (L). Data in (A) to (F) indicate mean ± SEM. (A to C) $n = 13$ to 15 mice per group; (D, E, and F) $n = 13$ (WT) and $n = 6$ (*Prdx1*$^{-/-}$). Donut charts in (G) and (L) show the mean proportion of cells expressing the indicated number of effector molecules. (G) $n = 13$ (WT) and $n = 6$ (*Prdx1*$^{-/-}$), (L) $n = 13$ to 15 per group; data representative of at least two independent experiments; (A to C) two-way ANOVA with Tukey's multiple comparisons test; (D to F) Mann-Whitney *U* test. *$P < 0.05$; **$P < 0.01$; ***$P < 0.001$; ****$P < 0.0001$; ns, not significant.

recycling, or pro-oxidant strategies that elevate ROS in the tumor environment. Notably, pharmacological ascorbate, which acts as a pro-oxidant at high concentrations, has demonstrated synergy with ICB in preclinical models (*56*–*58*), consistent with the concept that restoring ROS availability within tumors may enhance T cell–mediated antitumor immunity. The development of targeted strategies to disrupt extracellular antioxidant-mediated immunosuppression, while sparing systemic and cancer cell–intrinsic activity, may enable enhanced antitumor immunity and immunotherapy responses without increasing protumorigenic ROS signaling within cancer cells. The ability of T cells to both generate and sense extracellular peroxide also raises the possibility of paracrine ROS signaling, enabling immune cells to potentiate immune activation within tissue locales. Therapeutically modulating antioxidant capacity may therefore be further relevant to tuning T cell activation and limiting immunopathology in autoimmunity and infection (*59*–*63*).

REFERENCES AND NOTES

1. H. Kong, N. S. Chandel, *J. Biol. Chem.* **293**, 7499–7507 (2018).
2. M. Ogrunc *et al.*, *Cell Death Differ.* **21**, 998–1012 (2014).
3. C. M. Velicer, C. M. Ulrich, *J. Clin. Oncol.* **26**, 665–673 (2008).
4. E. D. Kantor, C. D. Rehm, M. Du, E. White, E. L. Giovannucci, *JAMA* **316**, 1464–1474 (2016).
5. E. A. Klein *et al.*, *JAMA* **306**, 1549–1556 (2011).
6. G. S. Omenn *et al.*, *N. Engl. J. Med.* **334**, 1150–1155 (1996).
7. D. Albanes *et al.*, *J. Natl. Cancer Inst.* **88**, 1560–1570 (1996).
8. G. E. Goodman *et al.*, *J. Natl. Cancer Inst.* **96**, 1743–1750 (2004).
9. D. O'Sullivan, D. E. Sanin, E. J. Pearce, E. L. Pearce, *Nat. Rev. Immunol.* **19**, 324–335 (2019).
10. P. C. Ho, S. M. Kaech, *Curr. Opin. Immunol.* **46**, 38–44 (2017).
11. E. N. Arner, J. C. Rathmell, *Cancer Cell* **41**, 421–433 (2023).
12. A. Sugiura, J. C. Rathmell, *J. Immunol.* **200**, 400–407 (2018).
13. R. D. Leone, J. D. Powell, *Nat. Rev. Cancer* **20**, 516–531 (2020).
14. L. A. Sena *et al.*, *Immunity* **38**, 225–236 (2013).
15. K. Pilipow *et al.*, *JCI Insight* **3**, e122299 (2018).
16. J. Chen *et al.*, *J. Immunol.* **212**, 258–270 (2024).
17. E. M. Steinert *et al.*, *Nat. Immunol.* **26**, 1267–1274 (2025).
18. N. E. Scharping *et al.*, *Nat. Immunol.* **22**, 205–215 (2021).
19. F. Vieceli Dalla Sega *et al.*, *Biochim. Biophys. Acta* **1843**, 806–814 (2014).
20. K. M. Holmström, T. Finkel, *Nat. Rev. Mol. Cell Biol.* **15**, 411–421 (2014).
21. M. Schieber, N. S. Chandel, *Curr. Biol.* **24**, R453–R462 (2014).
22. S. H. Jackson, S. Devadas, J. Kwon, L. A. Pinto, M. S. Williams, *Nat. Immunol.* **5**, 818–827 (2004).
23. I. F. Benzie, J. J. Strain, *Anal. Biochem.* **239**, 70–76 (1996).
24. E. R. Hoskins *et al.*, *PLOS ONE* **6**, e25056 (2011).
25. S. Li, R. Wang, M. Zhang, L. Wang, S. Cheng, *World J. Surg. Oncol.* **11**, 173 (2013).
26. M. M. Sklavos, H. M. Tse, J. D. Piganelli, *Free Radic. Biol. Med.* **45**, 1477–1486 (2008).
27. A. Östman, J. Frijhoff, A. Sandin, F. D. Böhmer, *J. Biochem.* **150**, 345–356 (2011).
28. S. R. Lee *et al.*, *J. Biol. Chem.* **277**, 20336–20342 (2002).
29. J. Kwon *et al.*, *EMBO J.* **24**, 2331–2341 (2005).
30. C. Cammann *et al.*, *Front. Immunol.* **13**, 958616 (2022).
31. J. Brockdorff, S. Williams, C. Couture, T. Mustelin, *Eur. J. Immunol.* **29**, 2539–2550 (1999).
32. J. A. Frearson, D. R. Alexander, *J. Exp. Med.* **187**, 1417–1426 (1998).
33. A. N. Macintyre *et al.*, *Immunity* **34**, 224–236 (2011).
34. K. Okkenhaug *et al.*, *Science* **297**, 1031–1034 (2002).
35. C. C. Wu *et al.*, *Mol. Cell. Proteomics* **9**, 1100–1117 (2010).
36. M. Di Pilato, R. Kfuri-Rubens, Yumm3.3 Mouse Model Time Course, Single Cell Portal, study SCP3022 (Broad Institute); https://singlecell.broadinstitute.org/single_cell/study/SCP3022/single-cell-transcriptomics-yumm3-3-model-di-pilato-lab-md-anderson-cancer-center.
37. L. Jerby-Arnon *et al.*, *Cell* **175**, 984–997.e24 (2018).
38. R. D. Schreiber, L. J. Old, M. J. Smyth, *Science* **331**, 1565–1570 (2011).
39. C. H. Tsai *et al.*, *Cell Metab.* **35**, 118–133.e7 (2023).
40. N. Riaz *et al.*, *Cell* **171**, 934–949.e16 (2017).
41. K. Meeth, J. X. Wang, G. Micevic, W. Damsky, M. W. Bosenberg, *Pigment Cell Melanoma Res.* **29**, 590–597 (2016).
42. C. H. Chang *et al.*, *Cell* **162**, 1229–1241 (2015).
43. P. C. Ho *et al.*, *Cell* **162**, 1217–1228 (2015).
44. M. R. Sullivan *et al.*, *eLife* **8**, e44235 (2019).
45. B. Perillo *et al.*, *Exp. Mol. Med.* **52**, 192–203 (2020).
46. M. Breau *et al.*, *JCI Insight* **4**, e127647 (2019).
47. K. Le Gal *et al.*, *Sci. Transl. Med.* **7**, 308re8 (2015).
48. H. Wang *et al.*, *Sci. Transl. Med.* **8**, 334ra51 (2016).
49. V. I. Sayin *et al.*, *Sci. Transl. Med.* **6**, 221ra15 (2014).
50. E. Piskounova *et al.*, *Nature* **527**, 186–191 (2015).
51. C. Wiel *et al.*, *Cell* **178**, 330–345.e22 (2019).
52. A. Singh *et al.*, *Clin. Cancer Res.* **27**, 877–888 (2021).
53. J. Härkönen *et al.*, *Redox Biol.* **61**, 102644 (2023).
54. K. C. Arbour *et al.*, *Clin. Cancer Res.* **24**, 334–340 (2018).
55. L. Mullen, E. M. Hanschmann, C. H. Lillig, L. A. Herzenberg, P. Ghezzi, *Mol. Med.* **21**, 98–108 (2015).
56. E. J. Campbell *et al.*, *Free Radic. Biol. Med.* **99**, 451–462 (2016).
57. O. K. Serrano *et al.*, *Free Radic. Biol. Med.* **87**, 193–203 (2015).
58. A. Magrì *et al.*, *Sci. Transl. Med.* **12**, eaay8707 (2020).

ACKNOWLEDGMENTS

The authors thank members of University of Cambridge Biomedical Services for technical support with animal experiments, members of the University of Cambridge School of Biological Sciences Flow Cytometry Facility for assistance with cell sorting and analysis, and members of the Babraham Institute Proteomics Department for assistance with mass spectrometry experiments. We apologize to those authors whose work we were unable to cite owing to space constraints. **Funding:** Medical Research Council grant MR/Y013301/1 (R.R., A.J.W.); MR/W018454/1 (R.R., J.Y.); MR/S024468/1 (R.R.); Wellcome Trust/Royal Society grant 105663/Z/14/Z (R.R., R.N., P.V.); ERC Consolidator Award EP/X024709/1 (R.R.); JSPS Overseas Research Fellowship (Y.Y.-K.); Cancer Research Institute (CRI) Lloyd J. Old STAR award 3914 (E.L.); Associazione Italiana per la Ricerca sul Cancro IG 2022–ID 27391 (E.L.); Medical Research Council UK MC_UU_00028/4 (M.P.M.). **Author contributions:** Conceptualization: A.J.W., A.M.P., R.R. Investigation: A.J.W., A.M.P., P.V., R.N., R.G., H.L., I.L., C.J., A.N., C.J.W., T.v.L., A.G.C., S.-F.T., L.D., A.C.E., S.K.W., Y.Y.-K., C.J.I., J.Y., I.M.G., J.C., A.A-D., M.P.M., A.M.J. Funding acquisition: B.S., E.L., L.F., K.O., P.-C.H., R.L.E., R.R. Project administration: B.S., R.L.E., R.R. Supervision: G.G., E.L., L.F., K.O., P.-C.H., R.L.E., R.R. Writing – original draft: A.J.W., A.M.P., R.R. Writing – review & editing: P.V., R.N., R.G., C.J.W., A.N., C.W., T.v.L., A.G.C., S.-F.T., L.D., A.C.E., S.K.W., Y.Y.-K., C.J.I., J.Y., I.M.G., J.C., A.A.-D., B.S., E.L., L.F., K.O., P.-C.H., R.L.E. **Competing interests:** R.R. is a scientific adviser to Enhanc3D Genomics and OligoTune Ltd and holds industrially funded collaborations with AstraZeneca PLC and F-Star Therapeutics on topics unrelated to this study. E.L. reports consulting fees from Swarm Oncology, Pfizer, Biolegend, Amgen, and Menarini and advisory board engagement from Gilead, all on topics unrelated to this study. The remaining authors declare no competing interests. **Data, code, and materials availability:** High-throughput sequencing data are available at NCBI GEO with accession numbers GSE335420 and GSE335418. Reanalyzed public datasets are detailed in the materials and methods and are available at GEO GSE115978, GSE91061, the Broad Institute Single Cell Portal (SCP3022), and via TIMER2.0 (TCGA). Custom code is available from the corresponding authors upon request (A.J.W., R.L.E., R.R.). Tumor lines and genetic constructs are available from the corresponding authors (A.J.W., R.L.E., R.R.) under a standard material transfer agreement.

SUPPLEMENTARY MATERIALS

science.org/doi/10.1126/science.adz8203
Materials and Methods; Figs. S1 to S11; References (*59*–*63*); Data S1 to S6

Submitted 23 June 2025; resubmitted 20 April 2026; accepted 2 July 2026
10.1126/science.adz8203

Tumor-derived antioxidants suppress immunity by depriving T cells of reactive oxygen species

Alexander J. Wesolowski, Ardon M. Pillay, Panagiota Vardaka, Rabab Nasrallah, Randy Greaves, Housaiyin Li, Iliana Loffreda, Chelsea Jenkin, Andrew M. James, Alica Nübling, Christopher J. Ward, Teresa von Linde, Alberto G. Conti, Sheue-Fen Tzeng, Layla Dahmani, Alexander C. Evans, Sarah K. Whiteside, Yumi Yamashita-Kanemaru, Charlotte J. Imianowski, Jie Yang, Ignacio Moraga Gonzalez, Jack Chapman, Aws Al-Deka, Klaus Okkenhaug, Michael P. Murphy, Bartlomiej Swiatczak, Geoffrey Guittard, Enrico Lugli, Lukas Flatz, Ping-Chih Ho, Robert L. Eil, and Rahul Roychoudhuri

Science **393** (6815), . DOI: 10.1126/science.adz8203

Editor's summary

Reactive oxygen species (ROS) have a paradoxical role in cancer. Low to moderate ROS levels can stimulate tumor growth, whereas excessive ROS accumulation triggers oxidative stress and DNA damage. Antioxidant therapies aim to neutralize free radicals and reduce oxidative stress, but clinical trials have not (yet) demonstrated improved cancer survival. Wesolowski *et al*. report that tumors can turn ROS dependency against the immune system, suppressing T cells and escaping antitumor immunity (see the Perspective by Chandel). Cancer cells secrete antioxidant enzymes, including peroxiredoxin 1 (PRDX1), into the extracellular space, depriving T cells of ROS needed for T cells to attack tumors effectively. Removing PRDX1 from cancer cells restored antitumor immunity and made otherwise resistant tumors sensitive to checkpoint blockade immunotherapy. These results suggest that targeting extracellular redox mechanisms could enhance the efficacy of immunotherapy. —Priscilla N. Kelly